Applied Catalysis B: Environmental 237 (2018) 409–415

Contents lists available at ScienceDirect

Applied Catalysis B: Environmental

journal homepage: www.elsevier.com/locate/apcatb

# Enhanced catalytic activity of electrodeposited Ni-Cu-P toward oxygen evolution reaction

Byung Keun Kim[a], Soo-Kil Kim[b], Sung Ki Cho[c,*], Jae Jeong Kim[a,*]

[a] School of Chemical and Biological Engineering, Seoul National University, Gwanak-gu, Seoul, 08826, South Korea
[b] School of Integrative Engineering, Chung-Ang University, Dongjak-gu, Seoul, 06974, South Korea
[c] Department of Chemical Engineering, Kumoh National Institute of Technology, Gumi-si, Gyeongsangbuk-do, 39177, South Korea

ARTICLE INFO

*Keywords:*
Nickel-copper-phosphorous
Oxygen evolution reaction (OER)
Electrodeposition
Electrocatalyst

ABSTRACT

The slow kinetics of the oxygen evolution reaction (OER) and the high cost of the precious metal catalysts for the OER limit the efficiency and cost-effectiveness of water splitting. In this study, we introduce electrodeposited nickel-copper-phosphorous (NiCuP) as an efficient OER electrocatalyst in alkaline medium. The addition of Cu into the NiP electrocatalyst significantly enhanced the OER activity. Optimization of the electrodeposition conditions revealed that $Ni_{59}Cu_{19}P_9$ in terms of atomic percent exhibited the best activity with a reduced Tafel slope and charge transfer resistance for the OER, compared to NiP. The $Ni_{59}Cu_{19}P_9$ catalyst successfully endured the OER operation at 10 mA/cm$^2$ for up to 30 h while maintaining a Faradaic efficiency of over 99%. The X-ray photoelectron spectroscopy showed that the amount of active Ni hydroxide (NiOOH) species increased with the addition of Cu, which likely contributed to the enhanced of catalytic activity.

## 1. Introduction

Electrochemical water splitting has been highlight as a promising strategy for efficient and large-scale hydrogen production due to its scalability and the high-purity hydrogen that can be produced [1–3]. Generally, the oxygen evolution reaction (OER) is thought to limit the overall water splitting rate since the reaction path of the OER involves four electrons and is more complicated than the hydrogen evolution reaction (HER) [4,5]. Electrochemical water splitting can be performed under either strong acidic or alkaline conditions, but alkaline electrolytes are preferred for the OER since it ensures better reaction kinetics and catalyst stability [6,7]. Although precious metal oxides such as iridium and platinum oxides exhibit outstanding performance as electrocatalysts for the OER, their high price limits the economic feasibility of the water splitting process [8,9].

To overcome cost concerns, earth-abundant first-row late transition metals such as Mn, Co, Ni, and Fe have attracted attention as promising OER electrocatalysts as their oxides exhibit good stability and high catalytic activity for the OER under alkaline conditions [2,3,10–18]. For Ni, its phosphides [19–30], sulfides [31–33], carbides [34–36], nitrides [37,38] and selenides [39–42] as well as oxides have been reported as effective OER catalysts. In particular, the OER catalytic performance of Ni-P has been extensively studied. Liu et al. [20] investigated the OER activity of an electrodeposited Ni-P nanoparticle film in addition to its HER activity, and used it as a bifunctional electrocatalyst for efficient water electrolysis. Stern et al. [22] recently demonstrated that $Ni_2P$ nanoparticles exhibit a high OER activity, which could be attributed to the core-shell structure of nickel phosphide/nickel oxide ($Ni_2P/NiO_x$) in the nanoparticle. Many studies on metal-phosphorous catalysts have reported that phosphorous introduced a partial positive charge to the active metal centers, resulting in increased activities [22–24]. Moreover, the P in $Ni_2P$ was reported to chemically support the outermost active $Ni(OH)_x$ layer, enhancing the stability of the catalyst [22].

Blending other elements into the electrocatalyst is an effective way to enhance the activity and stability of a catalyst. Many studies have reported that the addition of secondary elements leads to a shift in the surface electronic state and can enhance the catalytic activity towards the OER [19–23]. Burke et al. [43] reported the enhancement of the OER catalytic activity of NiOOH with Fe incorporation, which was attributed to an increase in the conductivity of NiOOH. In this study, Cu was chosen for incorporation into a Ni-P electrocatalyst towards the OER under alkaline conditions. A mixture of Ni and Cu readily forms a solid solution, and their interaction has already been extensively studied via X-ray diffraction (XRD) and X-ray photoelectron spectroscopy (XPS) analyses [44–47]. The addition of Cu to Ni has been reported to make it more oxidation-resistive [48], and enhance its performance for electrocatalytic oxidation of carbohydrates [49] and methanol [50].

* Corresponding authors.
*E-mail addresses:* chosk@kumoh.ac.kr (S.K. Cho), jjkimm@snu.ac.kr (J.J. Kim).

https://doi.org/10.1016/j.apcatb.2018.05.082
Received 6 December 2017; Received in revised form 29 April 2018; Accepted 28 May 2018
Available online 05 June 2018

Recently, Wei et al. [51] reported Ni-Cu-P (NiCuP) nano-foam as a bi-functional electrocatalyst for water splitting. This nano-foam was synthesized via the phosphorization of a Ni-Cu alloy, and its performance towards catalyzing the HER and OER was determined. Nevertheless, the role of Cu in Ni-based electrocatalyst has not been studied intensively and extensively. In this study, we investigated the OER activity of NiCuP under alkaline conditions with various elemental proportions in the electrocatalyst. The NiCuP electrocatalyst was directly synthesized via electrodeposition where its composition could be easily controlled by changing the concentration of metal precursor in the electrolyte. We evaluated and characterized the NiCuP electrocatalyst in terms of chemical state, catalytic activity, and its stability during the OER, as well as elucidated the role of Cu in the electrocatalyst.

## 2. Experimental

### 2.1. Preparation of the electrocatalysts

The NiCuP electrocatalyst was prepared via cathodic electrodeposition. A homemade Cu rotating disk electrode (RDE, Hunjin Mechanics) or Cu foil (250 μm thick, Alfa Aesar) were used as substrates for electrochemical and spectroscopic analysis, respectively, with a geometric area of 0.1257 $cm^2$ (4 mm diameter). Pt wire and a saturated calomel electrode (SCE, sat'd KCl, ALS) were used as a counter and reference electrode, respectively. The reference electrode was dipped in the electrolyte only during the measurement in order to prevent the cross-contamination of the electrolyte and KCl. As a pretreatment, the Cu electrode was washed with absolute ethanol then rinsed with deionized (DI) water to remove organic residues. Native oxides were removed by potential cycling from 0.0 to −1.5 V (vs. SCE, 20 mV/s) for 5 cycles in 0.1 M citric acid solution with a rotation of 1500 rpm. After oxide removal, DI water was used to wash off the residual citric acid. The solution for NiCuP electrodeposition was prepared with various concentrations of copper sulfate pentahydrate ($CuSO_4{\cdot}5H_2O$), nickel sulfate hexahydrate ($NiSO_4{\cdot}6H_2O$), and 0.5 M sodium hypophosphite ($NaH_2PO_2$) as sources of Cu, Ni, and P, respectively. The composition of the solution was modified from the solution previously used for CoP electrodeposition [23]. In addition, 0.15 M ethylenediamine ($C_2H_4(NH_2)_2$) was added to the solution and served as complexing agent. The total molar concentration of $Ni^{2+}$ and $Cu^{2+}$ source was fixed at 50 mM and the pH of the solution was adjusted to 10.40 by adding KOH or $H_2SO_4$. The detailed compositions of the solution and corresponding atomic ratio of the deposited catalysts, including nomenclature of the deposited electrocatalyst, are listed in Table 1, where the elemental ratio of each catalyst was obtained from quantitative XPS analysis (not shown). All of the materials were purchased from Sigma Aldrich and used without any further purification other than potassium hydroxide (KOH). Before electrodeposition of the electrocatalyst, the solution was purged for 20 min with 99.9% $N_2$ gas to remove dissolved oxygen in the solution. The electrocatalysts were electrodeposited with a two-step method. For the first step, −8 mA was applied for 1 s to initiate nucleation. Then, a constant potential of −1.711 V (vs. SCE) was applied until the total charge density reached 20 C/$cm^2$. During electrodeposition, the substrate (RDE or Cu foil) was rotated at 1500 rpm to enhance the mass transfer of metal precursors and to remove any hydrogen gas evolved during the deposition. After electrodeposition, the electrode was rinsed with DI water.

### 2.2. Characterization of the electrocatalysts

The surface morphology and the elemental composition of the electrodeposited electrocatalysts were analyzed using field-emission scanning electron microscopy (FE-SEM, Merlin Compact, Zeiss) and energy-dispersive X-ray spectroscopy (EDS, Merlin Compact, Zeiss), respectively. XPS (Sigma Probe, VG Scientific) measurements were conducted to investigate the chemical states of Ni, Cu, and P with a monochromatic 1486.6 eV movable Al Kα X-ray source. The obtained spectra were calibrated with the C 1s peak (binding energy 284.8 eV). The spectra were obtained with spherical sector analyzer with 275 mm diameter. Sample chamber was maintained at ultimate vacuum ($< 5 \times 10^{-10}$ bar). Survey scans were acquired with 400 μm spot size between the wide range of binding energies of 1–1200 eV. High-resolution scans with a < 1 eV resolution were obtained between 800 and 900 eV.

### 2.3. Electrochemical measurements

A three-electrode electrochemical cell was used to perform the electrochemical analyses. Pt wire and a saturated calomel electrode (SCE, sat'd KCl) were used as counter and reference electrodes, respectively. Before the measurement, the electrolyte was purged with 100 ccm 99.999% $N_2$ flow for 30 min. $N_2$ blowing was maintained at 100 ccm during the experiment. All electrochemical measurements were recorded with a PATSTAT™ MC potentiostat (Princeton Applied Research). The potentials were converted with respect to the reversible hydrogen electrode (RHE). Polarization curves were obtained in 1.0 M KOH solution (pH 14) in the potential range from 0.3–0.7 V (vs. SCE) on a NiCuP-electrodeposited RDE which was rotated at 2000 rpm. The solution resistance ($R_u$: 5.67 Ω) was compensated during the measurement. It is well known that Fe impurity from KOH solution is critical to the activity of Ni-based OER catalyst [52], and we thoroughly controlled the Fe impurity in this study. The Fe impurity level of KOH used in this study was less than 0.2 ppm. Moreover, the activity of NiCuP tested in KOH purified as described in Ref. [52]. was almost similar to that of NiCuP in unpurified KOH (Fig. S1), which indicated the effect of Fe impurity is insignificant in this study. The relative surface area of the NiCuP electrocatalyst was estimated from the double-layer charging capacitance ($C_{dl}$) and pseudo-capacitance, which are associated with the redox reaction of Ni oxide (see supporting information for further details regarding capacitance measurement). Chronopotentiometry (CP, 10 mA/$cm^2$) was performed for 30 h in a 1.0 M KOH solution with a 2000 rpm rotation to evaluate the long-term stability of the NiCuP electrocatalyst. Electrochemical impedance spectroscopy (EIS) was performed to measure the charge transfer resistance ($R_{ct}$) of the OER on the electrocatalysts. The frequency of AC signal varied from 100 kHz to 0.1 Hz with an amplitude of 10 mV, superimposed to the potentiostatic wave of 0.6 V (vs. SCE).

### 2.4. Gas chromatography measurements

Evolved oxygen gas was detected with an online gas chromatograph (GC, SERIES II Plus 5890, Hewlett Packard) connected to a gas-tight homemade electrochemical cell. He gas at a pressure of 20 psi and purity of 99.999% was used as a carrier gas during the GC measurement. A constant current of 10 mA for the OER was applied and the electrolyte solution was vigorously stirred throughout the experiment.

**Table 1**
Compositions of electrolytes and catalysts with various Ni:Cu:P ratio.

| Nomenclature | $Ni_{79}P_9$ | $Ni_{70}Cu_9P_9$ | $Ni_{59}Cu_{19}P_9$ | $Ni_{49}Cu_{29}P_9$ | $Ni_{36}Cu_{39}P_7$ | $Ni_{24}Cu_{48}P_4$ | $Ni_{14}Cu_{55}P_1$ |
|---|---|---|---|---|---|---|---|
| Ni:Cu:P (mM, in electrolyte) | 50:0:500 | 49.9:0.1:500 | 49.75:0.25:500 | 49.5:0.5:500 | 49:1:500 | 47.5:2.5:500 | 45:5:500 |
| Ni:Cu:P (at%, in catalyst) | 79:0:9 | 70:9:9 | 59:19:9 | 49:29:9 | 36:39:7 | 24:48:4 | 14:55:1 |

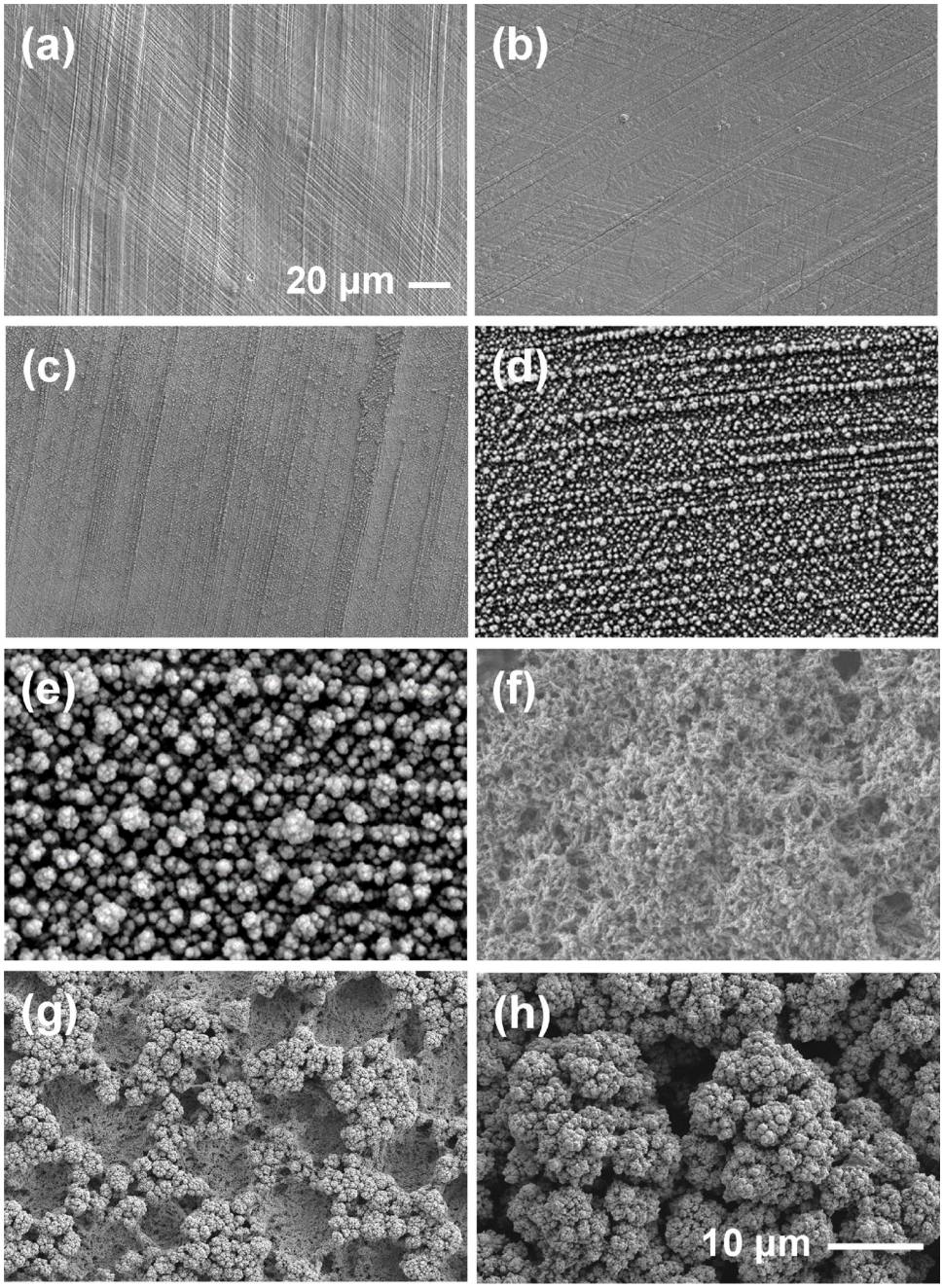


**Fig. 1.** Surface SEM images of (a) $Ni_{79}P_9$, (b) $Ni_{70}Cu_9P_9$, (c) $Ni_{59}Cu_{19}P_9$, (d) $Ni_{49}Cu_{29}P_9$, (e) $Ni_{36}Cu_{39}P_7$, (f) $Ni_{24}Cu_{48}P_4$, and (g–h) $Ni_{14}Cu_{55}P_1$ ((h): higher magnification).

During the measurement, gas was injected into the GC column every 3 min, and analyzed by a thermal conductivity detector (TCD).

## 3. Results and discussion

### 3.1. Characterization of the electrodeposited NiCuP film

While Ni, or more specifically, Ni oxide exhibits high catalytic activity toward the OER, NiP has been shown to have further enhanced activity [19–22,24–27], which was also observed in this study. The polarization curves for the OER on the electrodeposited NiP ($Ni_{79}P_9$) displayed a higher oxidation current and smaller Tafel slope, compared to pure Ni (Fig. S2). Fig. 1 shows the surface SEM images of the NiCuP electrocatalysts with various elemental composition. $Ni_{79}P_9$, $Ni_{70}Cu_9P_9$, and $Ni_{59}Cu_{19}P_9$ appeared to be very similar, whereas highly porous structures were observed with further addition of Cu. The atomic ratio of Cu in the electrocatalyst overwhelmed the concentration ratio of $Cu^{2+}$ in the electrolyte, which indicated that Cu deposition was more favorable than for the other metals. In the LSV (linear sweep voltammetry) for the $Cu^{2+}$ and $Ni^{2+}$ reduction, the current which was attributed to $Cu^{2+}$ reduction was clearly observed at the potential range from $-0.2$ to $-0.5$ V, whereas the current for $Ni^{2+}$ reduction did not emerge until hydrogen was evolved (Fig. S3). These results are consistent with the standard reduction potential value for Cu (0.340 V vs. NHE) which is more positive than for Ni ($-0.257$ V vs. NHE), though the actual potential would be shifted due to the presence of the complexing agent in the electrolyte. Since the NiCuP electrocatalyst was grown at $-1.7$ V (vs. SCE), $Cu^{2+}$ would be reduced under mass-transfer limiting conditions, and this may be the cause of the porous morphology of the Cu-rich NiCuP electrocatalysts. High-resolution EDS

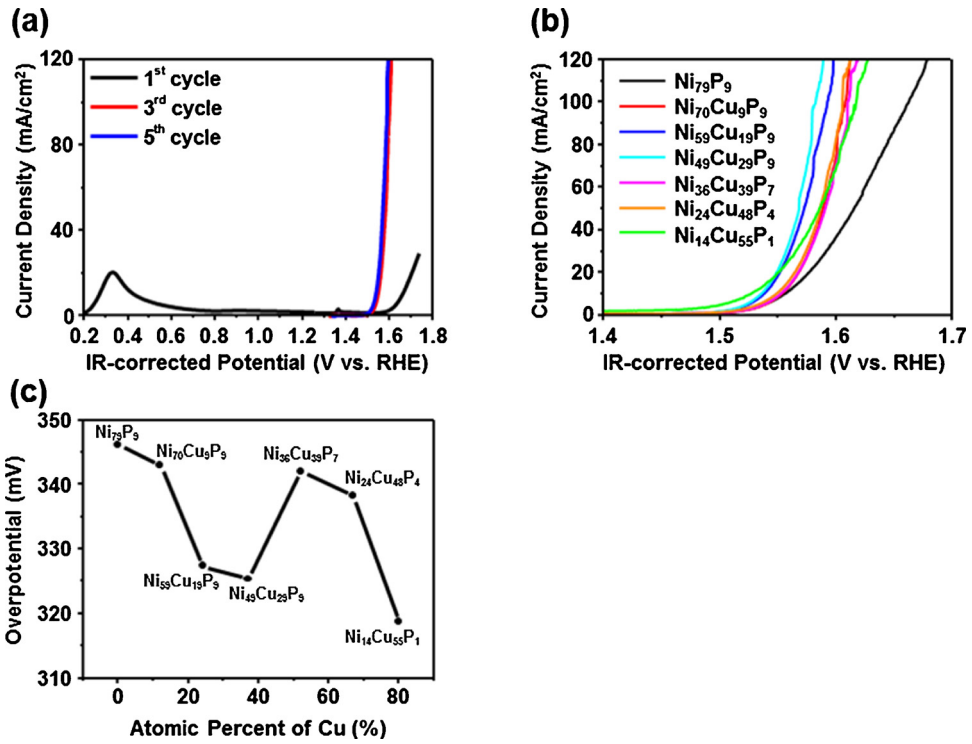


**Fig. 2.** (a) 1st, 3rd and 5th polarization curves of $Ni_{59}Cu_{19}P_9$, (b) polarization curves of NiCuP electrocatalysts with varying the concentration of Cu, and (c) overpotentials required for 10 mA/cm$^2$ current density for various NiCuP electrocatalyst. Measured current was divided by the geometric area (0.1257 cm$^2$) of the NiCuP deposited-electrode.

mapping of the electrocatalysts shows that the main elements (Ni, Cu, P, and O) are distributed uniformly throughout the surface (Fig. S4). For the XPS analyses of the as-prepared $Ni_{79}P_9$ and $Ni_{59}Cu_{19}P_9$, all deposited elements were found to be in the reduced state (Fig. S5). Ni predominantly exists as metallic Ni, giving rise to the peak at 852.8 eV, with some partially oxidized $NiO_x$ and Ni-P phase. The spectra of P indicated of the co-existence of P and $PO_x$ on the surface. Metallic Cu was also observed in the $Ni_{59}Cu_{19}P_9$. The P content, obtained from EDS analyses, did not vary significantly with the addition of up to 37% Cu, but it dramatically decreased when more than 52% Cu was added (Fig S6). As the concentration of hypophosphite as a source of P in the electrolyte was fixed in this study, the low P content in the Cu-rich NiCuP electrocatalyst might be due to the suppression of the P reduction and more limited incorporation of P on the Cu surface compared to Ni.

### 3.2. Evaluation of the electrocatalytic activity of NiCuP toward OER

The OER activities of the NiCuP electrocatalysts were examined with LSV. For the first scan, two oxidation peaks appeared at approximately 0.35 and 1.40 V (Fig. 2a). These oxidation peaks can be attributed to the oxidation of Ni to Ni(II) oxide and further to Ni(III) oxide (e.g. NiOOH), respectively. Previous studies [19–22] reported that Ni electrocatalysts require an activation step where the Ni electrocatalysts experience surface oxidation which increases their catalytic activity significantly, since the outermost NiOOH layer is credited as being essential for OER catalytic activity. Repeating the potential sweep in the positive direction gradually enhanced the catalytic activity, which then stabilized after 3–5 scans (Fig. 2a). Accordingly, the catalytic activity of each electrocatalyst was evaluated after 5 potential scans as an activation step. The polarization curves of the various ratios of Ni/Cu for the NiCuP electrocatalysts are shown in Fig. 2b. The current for the OER clearly increased with the addition of Cu to the NiP. However, the synergetic effect of Cu was not observed when phosphorous was not contained in the electrocatalyst (Fig. S7), which is consistent with the observation of the deteriorating effect of Cu on the OER activity of Ni hydroxide [52]. Fig. 2c shows the overpotential required to deliver 10 mA/cm$^2$ for each electrocatalyst, but there was no clear correlation between the catalytic activity and Cu content. $Ni_{14}Cu_{55}P_1$ exhibited the lowest overpotential (318.7 mV) at 10 mA/cm$^2$ for the OER but its polarization curve had a somewhat gentle slope. In addition, its capacitive current was relatively large (Fig. 2c), which indicates a relatively high surface area. Accordingly, the low overpotential at a given current density of $Ni_{14}Cu_{55}P_1$ likely originates from its high surface area.

The variation in the surface area according to the addition of Cu after the activation step was investigated through the measurement of the double-layer charging current ($i_c = AC_{dl}\nu$, A: surface area, $C_{dl}$: double-layer capacitance, $\nu$: scan rate) and the charge for pseudo-capacitance of the Ni oxide (or hydroxide). Fig. 3a shows typical non-Faradaic region voltammograms of the NiCuP electrocatalysts at a 200 mV/s scan rate, which showed that the charging current increased with the atomic concentration of Cu. Assuming that $C_{dl}$ is constant over all NiCuP electrocatalysts tested, the charging current is proportional to the surface area, and the results indicate an increase in the surface area, which is consistent with the change in the surface morphology (Figs. 1a and S4). The difference in the surface area was also verified by pseudo-capacitance measurement of the Ni oxide (or hydroxide) where the total charge consumed for the phase transition is proportional to electrochemically active surface area. The current peak and the corresponding charge also increased with the concentration of Cu (Fig. 3b). The relative surface area of each electrocatalyst with respect to that of the $Ni_{79}P_9$ catalyst was estimated from the capacitance data and shown in Fig. 3c. While the surface areas of $Ni_{70}Cu_9P_9$ and $Ni_{59}Cu_{19}P_9$ were similar to that of $Ni_{79}P_9$, they became larger with the further addition of Cu. Both measurements showed a similar trend, but the surface area estimated from $C_{dl}$ was larger than that obtained from the pseudo-capacitance. This is likely because the Ni oxide peak area solely depends on the amount of Ni located on surface, whereas $C_{dl}$ is influenced by all the elements on the surface. From both capacitance measurements, the surface area was quantified and was consistent with results from the qualitative observation of the surface morphologies in Fig. 1.

The polarization curves were normalized to the surface area of the catalyst calculated from $C_{dl}$ and shown in Fig. 4a, which clearly shows the effect of Cu on catalytic activity independently on the change in

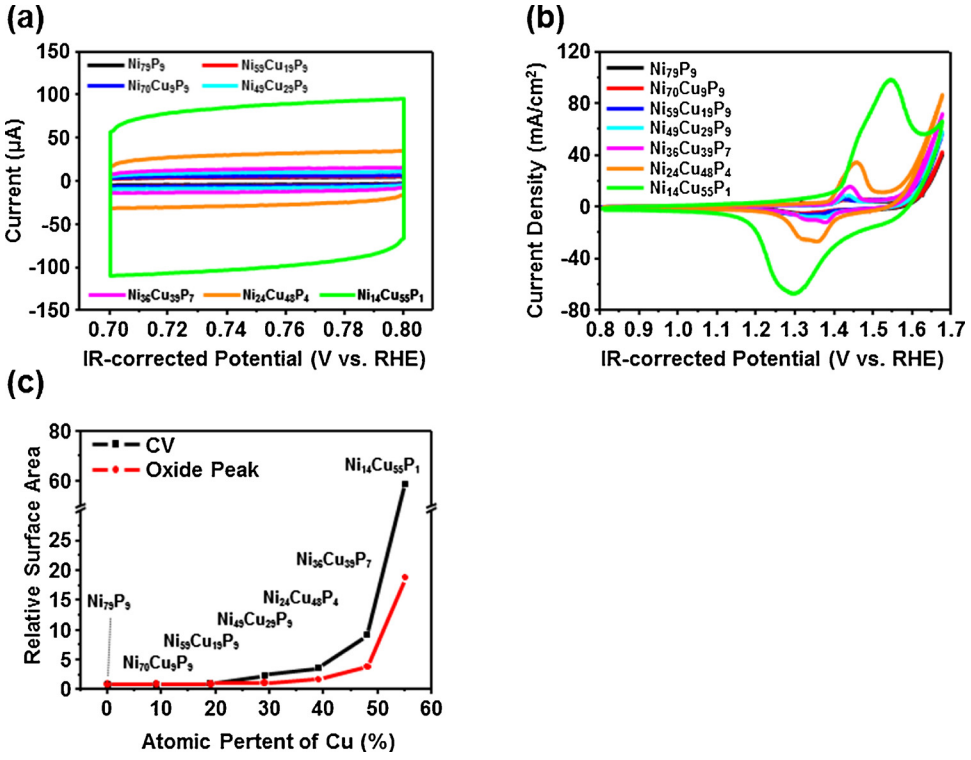


**Fig. 3.** Cyclic voltammograms for various NiCuP electrocatalysts, measured at 200 mV/s scan rate (a) in non-Faradaic potential region and (b) in the potential range for the surface redox reaction of $NiO_x$. (c) The plot of the relative surface area against the atomic concentration of Cu. The relative surface area with respect to that of $Ni_{79}P_9$ was estimated from double-layer charge capacitance and pseudocapacitance of NiCuP electrocatalyst.

surface area. Per unit of surface area, $Ni_{59}Cu_{19}P_9$ exhibited the best OER performance while $Ni_{14}Cu_{55}P_1$ was less active than $Ni_{79}P_9$. The overpotential required to deliver 10 mA/cm$^2$ of current density was 307 mV for $Ni_{59}Cu_{19}P_9$ and 326 mV for $Ni_{79}P_9$. In the Tafel analysis (Fig. 4b and c), the slope decreased with the addition of Cu, was minimized for $Ni_{59}Cu_{19}P_9$, and then increased again with increasing Cu concentration. The exchange current density ($j_0$) was maximized at $Ni_{59}Cu_{19}P_9$. The superior OER performance of $Ni_{59}Cu_{19}P_9$ was also confirmed by the small charge transfer resistance measured via EIS analysis (Fig. S8). The Nyquist plots clearly show that $Ni_{59}Cu_{19}P_9$ has smaller semicircle compared to $Ni_{79}P_9$ where the charge transfer resistances were estimated to be 121.7 ( ± 7.4) and 201.9 ( ± 15.9) Ω/cm$^2$ at 1.67 V (vs. RHE), respectively.

The enhanced oxygen evolution was confirmed with chronopotentiometry and gas chromatography. As show in Fig. 5a, a lower initial overpotential (293 mV) was required to achieve 10 mA/cm$^2$ for the OER with $Ni_{59}Cu_{19}P_9$ compared to $Ni_{79}P_9$ (314 mV), and there was no significant overpotential increase over 30 h of operation, which indicates the stable operation of $Ni_{59}Cu_{19}P_9$. For $Ni_{14}Cu_{55}P_1$, the overpotential was initially low, which was due to its high surface area, but

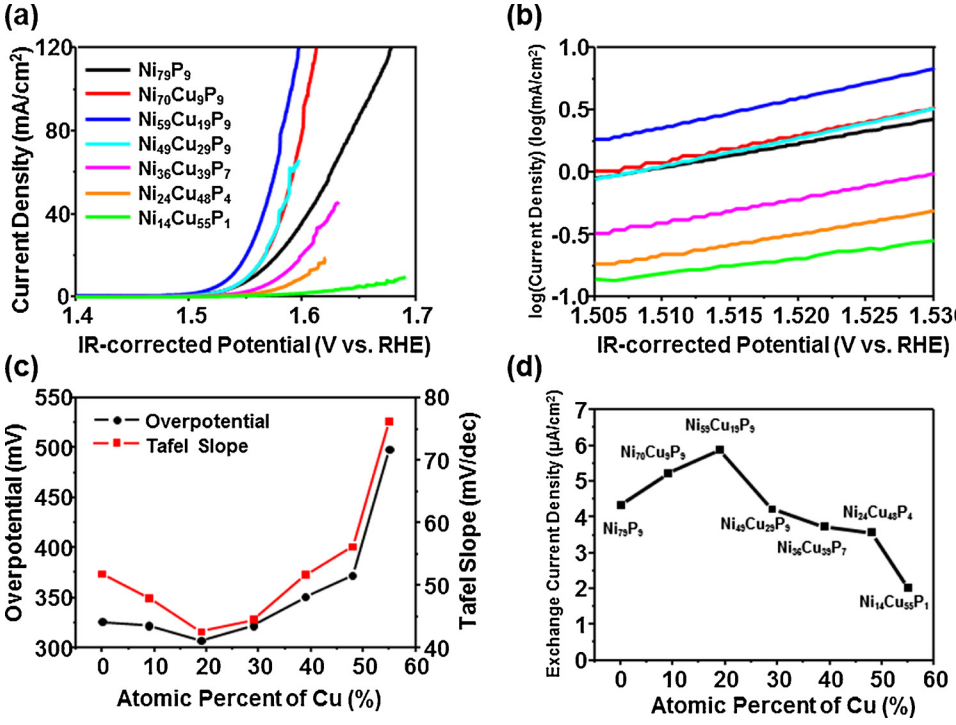


**Fig. 4.** (a) Surface area-normalized polarization curves, assuming that the microscopic area of $Ni_{79}P_9$ was equal to the geometric area, (b) Tafel plots of various NiCuP electrocatalysts, (c) the variation of Tafel slopes and overpotentials (for 10 mA/cm$^2$), and (d) exchange current density of NiCuP electrocatalysts according to the concentration of Cu.

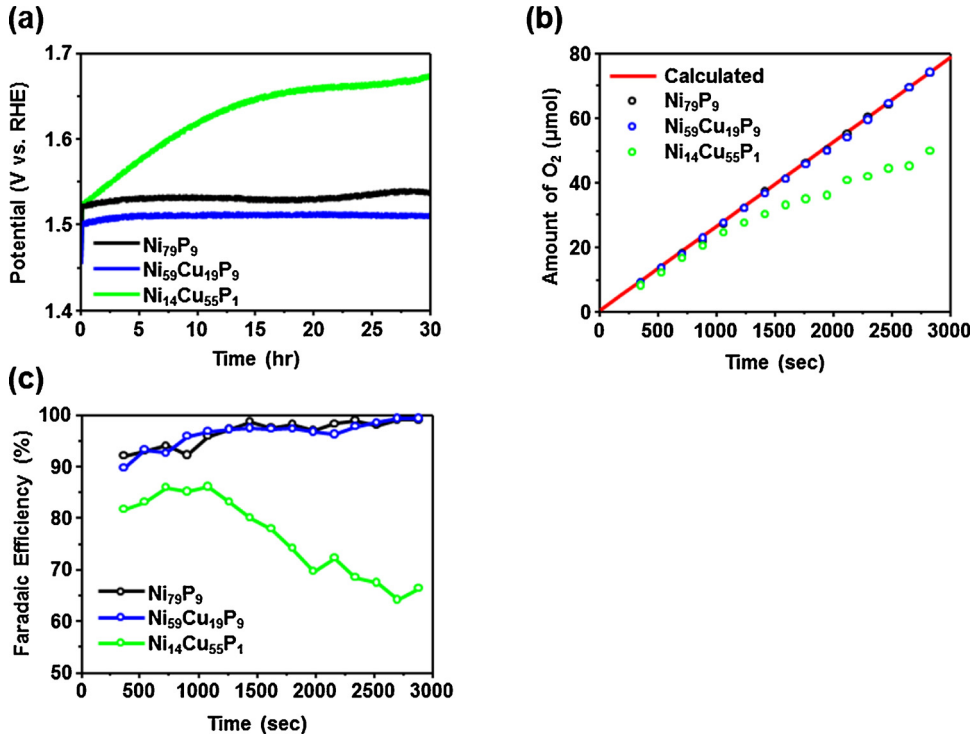


**Fig. 5.** (a) Chronopotentiogramms of $Ni_{79}P_9$, $Ni_{59}Cu_{19}P_9$, and $Ni_{14}Cu_{55}P_1$ for 30 h, (b) The amount of evolved oxygen gas, and (c) Faradaic efficiency measured during chronopotentiometry.

then increased gradually. GC measurements (see Supporting information for the detailed experimental set-up, Fig. S9) of the $Ni_{79}P_9$ and $Ni_{59}Cu_{19}P_9$ verified that the evolved oxidation current was attributed to the OER, whereas side-reactions such as surface oxidation, occurred on $Ni_{14}Cu_{55}P_1$ (Fig. 5b). Although the Faradaic efficiency for the OER with $Ni_{59}Cu_{19}P_9$ was initially low (~90%) due to the surface oxidation of the electrocatalyst, it reached nearly 100% (99.18%) after 51 min (Fig. 5c). The polarization curve of $Ni_{59}Cu_{19}P_9$ after 30 h of OER operation did not change significantly (Fig. S10b and e) whereas $Ni_{14}Cu_{55}P_1$ suffered from significant performance degradation with regard to the oxidation current and Tafel slope (Fig. S10c and f). These results were consistent with chronopotentiometric experiment (Fig. 5a). As previously mentioned, P in the electrocatalyst supports the upper NiOOH layer, whereby the low stability of $Ni_{14}Cu_{55}P_1$ might be related to its low P content.

### 3.3. Exploration of the role of the Cu in NiCuP electrocatalyst

To investigate the catalytic enhancement that occurred with the addition of Cu, high-resolution XPS analyses were performed on the NiCuP electrocatalysts. Casella et al. [53] observed the increase in the amount of NiOOH on Au-supported Ni hydroxide layer via XPS analyses. Fig. 6 shows the Ni $2p_{3/2}$ spectra of the activated NiCuP electrocatalysts with various Cu concentrations. After activation, the Ni metallic peaks shown in Fig. S4 disappeared, and the $NiO_x$ peak became predominant. The peak corresponding to $Ni^{3+}$ (green curve) was also found on the surface, and corresponds to NiOOH. It is clear that the peak was present at low Cu concentrations although it became negligible at higher Cu concentration (> 39 at.%). As mentioned above, the outermost NiOOH layer is credited for the OER activity of the catalyst [21,22,24], whereby the variation of the catalytic activity of the NiCuP is closely associated with the amount of NiOOH in the electrocatalyst. As the Cu content increases above 39%, another metallic peak of Ni appears at 853.8 eV, which was also found even after 30 h of operation (Fig. S11). This indicates that some Ni atoms in the $Ni_{14}Cu_{55}P_1$ were not involved in the OER catalysis, and it is likely that the Cu surrounding Ni in the electrocatalyst layer blocks the active Ni OER site. The ratio of $Ni^{3+}$ to the total amount of Ni species in the activated NiCuP electrocatalyst was plotted as a function of atomic concentration of Cu (Fig. 7). It increased gradually with the addition of Cu and formed a maximum at the composition of $Ni_{59}Cu_{19}P_9$, and subsequently decreased with increasing Cu content. The same trend was observed for the electrocatalyst operated for 30 h (Fig. S11) and it matched well with the activity plot (Fig. 4c and d). These results indicate that the addition of Cu to the NiCuP electrocatalyst increases the amount of NiOOH present and accordingly enhances the catalytic activity. Hameed et al. [50] reported that β-NiOOH, which is the active $Ni^{3+}$ species, can be stabilized by the addition of Cu (Cu hydroxide specifically) to Ni hydroxide as an electrocatalyst for methanol oxidation. The enhancement of the OER activity of the NiCuP electrocatalyst can be understood in the same way, and is supported by the XPS analyses presented herein.

## 4. Conclusions

A NiCuP electrocatalyst was successfully synthesized via cathodic electrodeposition, and it showed higher performance toward the OER compared to NiP. Its catalytic activity was maximized at the atomic composition of $Ni_{59}Cu_{19}P_9$ with a Tafel slope value of 42.5 mV/dec and overpotential of 307 mV for the current density of 10 $mA/cm^2$. GC analysis verified that enhanced oxygen evolution was achieved with almost 100% Faradaic efficiency. XPS analysis revealed that the introduction of Cu into NiP increased the amount of $Ni^{3+}$ species, which likely was the driving force behind the higher catalytic activity.

## Declarations of a competing interest

The authors declare no competing financial interest.

## Acknowledgments

This research was supported by the Technology Innovation Program (10043789) funded by the Ministry of Knowledge Economy (MKE,

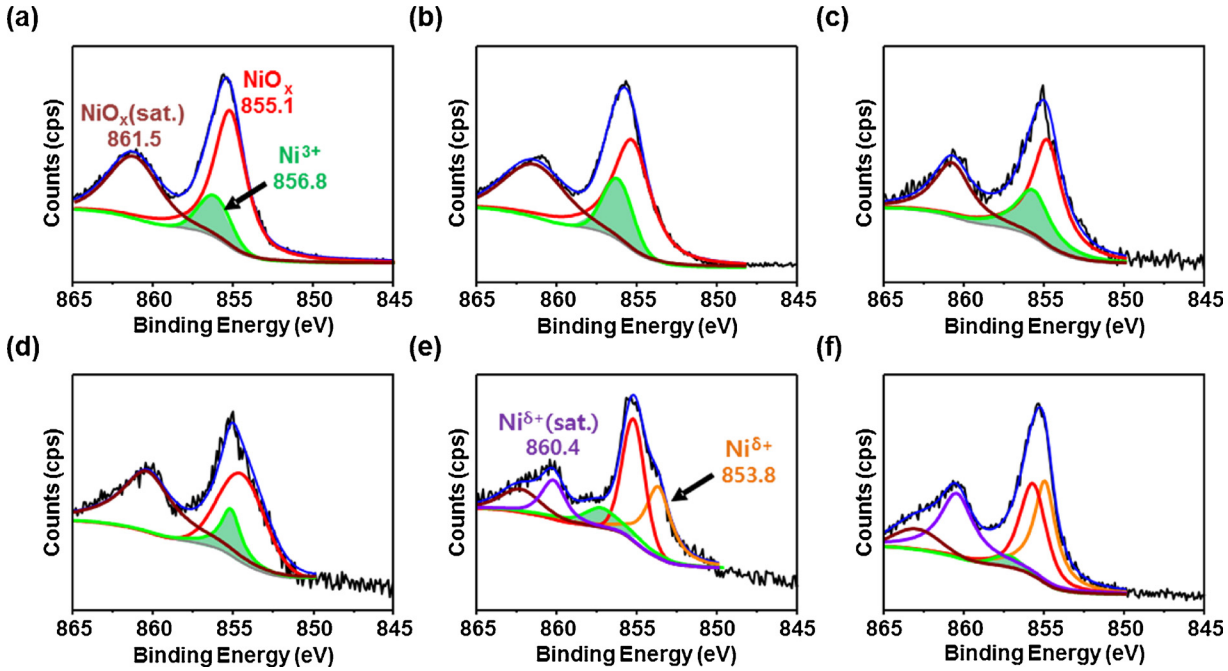


**Fig. 6.** High-resolution Ni $2p_{3/2}$ spectra shown for the activated (a) $Ni_{79}P_9$, (b) $Ni_{70}Cu_9P_9$, (c) $Ni_{59}Cu_{19}P_9$, (d) $Ni_{49}Cu_{29}P_9$, (e) $Ni_{36}Cu_{39}P_7$, and (f) $Ni_{24}Cu_{48}P_4$.

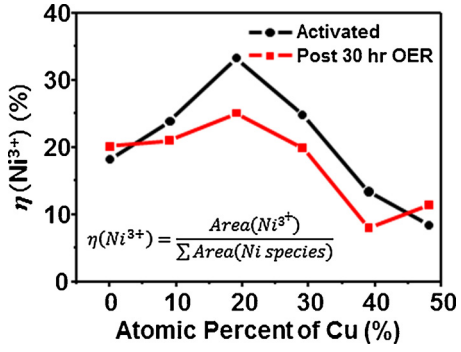


**Fig. 7.** The proportion of $Ni^{3+}$ peak out of entire Ni species for NiCuP electrocatalysts with various atomic concentration of Cu.

Korea), and the Basic Science Research Program through the National Research Foundation of Korea (NRF) funded by the Ministry of Science, ICT & Future Planning (NRF-2015R1C1A1A02037791).

## Appendix A. Supplementary data

Supplementary material related to this article can be found, in the online version, at doi:https://doi.org/10.1016/j.apcatb.2018.05.082.

## References

[1] S. Chu, A. Majumdar, Nature 488 (2012) 294–303.
[2] I. Roger, M.A. Shipman, M.D. Symes, Nat. Rev. Chem. 1 (2017) 1–12.
[3] S. Anantharaj, S.R. Ede, K. Sakthikumar, K. Karthick, S. Mishra, S. Kundu, ACS Catal. 6 (2016) 8069–8097.
[4] A.J. Bard, M.A. Fox, Acc. Chem. Res. 28 (1995) 141–145.
[5] H. Dau, C. Limberg, T. Reier, M. Risch, S. Roggan, P. Strasser, ChemCatChem 2 (2010) 724–761.
[6] R.L. LeRoy, Int. J. Hydrogen Energy 8 (1983) 401–417.
[7] K. Zeng, D. Zhang, Prog. Energy Combust. 36 (2010) 307–326.
[8] T. Reier, M. Oezaslan, P. Strasser, ACS Catal. 2 (2012) 1765–1772.
[9] M. Carmo, D.L. Fritz, J. Merge, D.A. Stolten, Int. J. Hydrogen Energy 38 (2013) 4901–4934.
[10] M.D. Kärkäs, B. Akermark, Dalton Trans. 45 (2016) 14421–14461.
[11] A. Mills, Chem. Soc. Rev. 18 (1989) 285–316.
[12] M. Gong, H. Dai, Nano Res. 8 (2015) 23–39.
[13] L. Trotochaud, J.K. Ranney, K.N. Williams, S.W. Boerttcher, J. Am. Chem. Soc. 134 (2012) 17253–17261.
[14] M.E.G. Lyons, M.P. Brandon, J. Electroanal. Chem. 641 (2010) 119–130.
[15] H.J. Miao, D.L. Piron, J. Appl. Electrochem. 21 (1991) 55–59.
[16] X. Li, F.C. Walsh, D. Pletcher, Phys. Chem. Chem. Phys. 13 (2011) 1162–1167.
[17] A. Singh, S.L.Y. Chang, R.K. Hocking, U. Bach, L. Spiccia, Energy Environ. Sci. 6 (2013) 579–586 9NI.
[18] B.C.M. Martindale, E. Reisner, Adv. Energy Mater. 6 (2016) 1502095.
[19] X. Wang, W. Li, D. Xiong, D.Y. Petrovykh, L. Liu, Adv. Funct. Mater. 26 (2016) 4067–4077.
[20] Q. Liu, S. Gu, C.M. Li, J. Power Sources 299 (2015) 342–346.
[21] X. Wang, W. Li, D. Xiong, L. Liu, J. Mater. Chem. A 4 (2016) 5639–5646.
[22] L. Stern, L. Feng, F. Song, X. Hu, Energy Environ. Sci. 8 (2015) 2347–2351.
[23] N. Jiang, B. You, M. Sheng, Y. Sun, Angew. Chem. Int. Ed. 54 (2015) 6251–6254.
[24] B. You, N. Jiang, M. Sheng, M.W. Bhushan, Y. Sun, ACS Catal. 6 (2016) 714–721.
[25] A. Han, H. Chen, Z. Sun, J. Xu, P. Du, Chem. Commun. 51 (2015) 11626–11629.
[26] Jiayuan Li, Jing Li, X. Zhou, Z. Xia, W. Gao, Y. Ma, Y. Qu, ACS Appl. Mater. Interfaces 8 (2016) 10826–10834.
[27] M. Ledendecker, S.K. Calderon, C. Papp, H. Steinruck, M. Antonietti, M. Shalom, Angew. Chem. Int. Ed. 54 (2015) 12361–12365.
[28] N. Jiang, B. You, M. Sheng, Y. Sun, ChemCatChem 8 (2016) 106–112.
[29] P.W. Menezes, A. Indra, C. Das, C. Walter, C. Gobel, V. Gutkin, D. Schimeiber, M. Driess, ACS Catal. 7 (2016) 103–109.
[30] A. Han, H. Zhang, R. Yuan, H. Ji, P. Du, ACS Appl. Mater. Interfaces 9 (2016) 2240–2248.
[31] J. Chang, Q. Lv, G. Li, J. Ge, C. Liu, W. Xing, Appl. Catal. B 204 (2017) 486–496.
[32] W. Zhou, X.-J. Wu, X. Cao, X. Huang, C. Tan, J. Tian, H. Liu, J. Wang, H. Zhang, Energy Environ. Sci. 6 (2013) 2921–2924.
[33] T. Liu, Y. Liang, Q. Liu, X. Sun, Y. He, A.M. Asiri, Electrochem. Commun. 60 (2015) 92–96.
[34] P. Ganesan, M. Prabu, J. Sanetuntikul, S. Shanmugam, ACS Catal. 5 (2015) 3625–3637.
[35] H. Yang, S. Luo, X. Li, S. Li, J. Jin, J. Ma, J. Mater. Chem. A 4 (2016) 18499–18508.
[36] T.Y. Ma, J.L. Cao, M. Jaroniec, S.Z. Qiao, Angew. Chem. Int. Ed. 55 (2016) 1138–1142.
[37] A. Pendashteh, J. Palma, M. Anderson, R. Marcilla, Appl. Catal. B 201 (2017) 241–252.
[38] S. Cai, Z. Meng, H. Tang, Y. Wang, P. Tsiakaras, Appl. Catal. B 217 (2017) 477–484.
[39] Xiang Xu, F. Song, Xile Hu, Nat. Commun. 7 (2016) 12324.
[40] A.T. Swesi, J. Masud, M. Nath, Energy Environ. Sci. 9 (2016) 1771–1782.
[41] Z. Pu, Y. Luo, A.M. Asiri, X. Sun, ACS Appl. Mater. Interfaces 8 (2016) 4718–4723.
[42] A. Sivanantham, S. Shanmugam, Appl. Catal. B 203 (2017) 485–493.
[43] M.S. Burke, M.G. Kast, L. Trotochaud, A.M. Smith, S.W. Boettcher, J. Am. Chem. Soc. 137 (2015) 3638–3648.
[44] G.K. Wertheim, S. Hüfner, H.J. Guggenheim, Phys. Rev. B 7 (1973) 556–558.
[45] S. Hüfner, G.K. Wertheim, Phys. Rev. B 7 (1973) 2333–2335.
[46] G.K. Wertheim, H.J. Guggenheim, S. Hüfner, Phys. Rev. Lett. 30 (1973) 1050–1053.
[47] A.R. Nagahash, T.H. Etsell, S. Xu, Chem. Mater. 18 (2006) 2480–2488.
[48] T. Doi, Y. Nichiyama, A. Yoshigoe, Y. Teraoka, Surf. Interface Anal. 48 (2016) 685–688.
[49] I.G. Casella, M. Gatta, J. Electrochem. Soc. 149 (2002) B465–B471.
[50] R.A.A. Hameed, K.M. El-Khatib, Int. J. Hydrogen Energy 35 (2010) 2517.
[51] L. Wei, K. Goh, O. Birer, H.E. Karahan, J. Chang, S. Zhai, X. Chen, Y. Chen, Nanoscale 9 (2017) 4401–4408.
[52] O. Diaz-Morales, I. Ledezma-Yanez, M.T.M. Koper, F. Calle-Vallejo, ACS Catal. 5 (2015) 5380–5387.
[53] I.G. Casella, M.R. Guascito, M.G. Sannazzaro, J. Electroanal. Chem. 462 (1999) 202–210.